Electrochimica Acta 506 (2024) 144994

Contents lists available at ScienceDirect

Electrochimica Acta

journal homepage: www.journals.elsevier.com/electrochimica-acta

Enhancement of ionic conductivity in electrically conductive membranes by polarization effect

Ivan A. Kharchenko [a,b], Nikita V. Vaulin [c], Mikhail M. Simunin [a,d], Semen A. Mareev [e], Ivan V. Nemtsev [b,d], Alexandr S. Goltaev [c], Denis V. Lebedev [c,f], Ilya I. Ryzhkov [a,b,*]

[a] Institute of Computational Modelling SB RAS, Akademgorodok 50–44, 660036 Krasnoyarsk, Russia
[b] Siberian Federal University, Svobodny 79, 660041 Krasnoyarsk, Russia
[c] St. Petersburg Academic University, 8/3 Khlopina St., 194021 St. Petersburg, Russia
[d] Federal Research Center KSC SB RAS, Akademgorodok 50–38, 660036 Krasnoyarsk, Russia
[e] Kuban State University, Stavropolskaya St. 149, 350040 Krasnodar, Russia
[f] Institute for Analytical Instrumentation RAS, 31–33 Ivana Chernykh St., 190103 St. Petersburg, Russia

ARTICLE INFO

Keywords:
Nanopore
Ionic conductivity
Polarization
Porous anodic alumina membrane
Carbon nanotubes
Modeling

ABSTRACT

Electrically conductive nanoporous membranes represent a class of stimuli–responsive materials, which selectivity/permeability characteristics can be adjusted by varying the surface potential. In this work, we perform a comprehensive theoretical and experimental study of ionic conductivity of such membranes. The 2D Space charge and 1D Uniform potential models are used to describe the ion transport through a cylindrical nanopore. The calculations show that the imposed electric field polarizes the conductive surface, which results in the continuous variation of electronic surface charge from positive to negative along the nanopore. A higher concentration of cations (anions) is observed at negatively (positively) charged part of the nanopore. The increase of charge carries concentration due to polarization effect results in the enhancement of ionic conductivity with increasing the voltage difference. The corresponding current–voltage curves are non-linear. The enhancement can reach a few orders of magnitude at low salt concentrations, but becomes much smaller at high concentrations. The presence of chemical charge has a screening effect on the interaction of electric field with the electronic charge on the nanopore surface, and reduces the conductivity enhancement. A novel analytical solution is derived for the dependence of ionic current on the Stern layer capacitance, salt concentration, and the applied potential difference. The theoretical predictions are first confirmed by the ionic conductivity measurements in porous anodic alumina membranes with carbon nanotubes inside the pores. The experimental data are approximated by the 1D Uniform potential model curves using chemical charge as a fitting parameter. Strong enhancement of ionic conductivity (more than 6 times) and the corresponding non-linear dependence of current on the applied voltage is experimentally registered at low KCl concentrations (0.1 – 10 mM) with increasing the voltage difference.

1. Introduction

In recent decades, many research groups have focused their attention on the development and investigation of stimuli–responsive membranes [1]. Such membranes can change their transport properties in response to external signals (changes in temperature, light, electric field, ionic strength, and pH) [2,3]. Electrically conductive membranes represent a class of stimuli–responsive materials, which provide the possibility of varying their surface charge by applying a prescribed potential [4]. The electrostatic interaction between membrane surface and charged components (ions) gives a powerful tool for control and adjustment of membrane selectivity, conductivity, and rejection [5,6].

Switching the ionic selectivity from cation to anion by varying the surface potential was first demonstrated for track-etched membranes with gold coating of pores [7,8]. The control of ion diffusion fluxes through track–etched as well as carbon black membranes was achieved by changing the applied potential in [9,10]. One of the first applications of conductive membranes to nanofiltration was presented in [11]. Using a membrane based on nanotubes and conducting polymers, the authors demonstrated the increase of rejection for monovalent ions from 50% to 80% without decreasing the liquid permeability. Similar results were obtained on the basis of membranes with a selective layer from nanotubes and graphene oxide [12]. The increase of dye rejection

* Corresponding author at: Institute of Computational Modelling SB RAS, Akademgorodok 50–44, 660036 Krasnoyarsk, Russia.
E-mail address: rii@icm.krasn.ru (I.I. Ryzhkov).

https://doi.org/10.1016/j.electacta.2024.144994
Received 12 June 2024; Received in revised form 28 August 2024; Accepted 30 August 2024
Available online 4 September 2024

by MXene/CNT nanofiltration membrane was achieved by applying cathode potential to the membrane surface in [13].

To understand and predict complex ion transport mechanisms in conductive membranes, mathematical models are widely employed. The capillary models assume that the membrane can be represented as an array of cylindrical pores, and consider the ion transport through a single pore [14]. The classical 2D Space charge (SC) model [15] and its 1D analogue known as Uniform potential (UP) model [16] were originally developed for nanopores with constant surface charge density. These models were applied to the analysis of electrokinetic phenomena [17], determination of zeta potential [18], membrane potential at zero current [19] as well as carbon nanotube conductivity [20]. The SC and UP models were revisited in [21,22] and later extended to the case of conductive nanopores with constant surface potential in [23]. The experimental results on switchable ionic selectivity were described by the extended models in [24,25]. A new effect of enhancing the membrane potential at zero current due to polarization of conductive surface by the electric field caused by ions diffusion was discovered in [26]. The polarization induces an inhomogeneous electronic charge on the conductive surface, which can trigger various phenomena such as electroosmotic flows [27,28] or bipolar currents between cathodic and anodic parts of the surface in the presence of a reversible redox couple [29]. Thus, the key difference between non-conductive and conductive surfaces is that the latter can developed polarization (or induced) charges in the presence of electric field. The model, which takes into account the induced electronic and pH–dependent chemical surface charges, was proposed in [30]. It was based on the theory of amphifunctional interfaces allowing both electronic and ionic surface charging [31,32]. The extension of UP model to describe nanofiltration of binary aqueous electrolytes with the help of electrically conductive membranes was proposed in [33] and applied to describing the experimental results obtained in [11,13].

The ability of nanopores to transport ions under the applied electric field is characterized by the ionic conductivity. There have been a number of studies of ionic conductance in electrically conductive membranes and single nanochannels. The authors of [34] found that the increase of applied potential magnitude resulted in the enhancement of ionic conductivity in gold nanotube membranes due to increase of counter-ion concentration in the pores. However, it was found that the adsorption of ions on the pore surface at anodic potential vanished the conductivity enhancement effect. The increase of pure water conductivity by a few orders of magnitude by varying the potential of a porous gold membrane was discovered in [35]. Using alumina nanofiber membrane with conductive carbon coating, the authors of [36] demonstrated the change of its ionic conductivity and selectivity by changing the surface potential. The principle of electrostatic gating was also employed for control of ionic conduction in field-effect reconfigurable ionic diodes [37]. The study of graphene nanopores showed that their ionic conductivity spans three orders of magnitude, and they display distinct linear, voltage-activated or rectified current–voltage characteristics [38]. The ionic current measurements through several single-walled nanotubes were reported in [39]. Linear and nonlinear current–voltage dependencies were observed. The latter were explained theoretically by local energy barriers along the nanopores (i.e. regions without surface charge). The voltage-gated nanochannels, where both the potential applied to the conductive membrane surface and the transmembrane potential are independently controlled, were theoretically analyzed in [40]. Using 2D numerical modeling based on the Navier–Stokes, Nernst–Planck, and Poisson equations, the authors showed that transmembrane potential induces an inhomogeneous charge distribution on the nanochannel surface, which can affect its ionic conductivity. Modeling the effect of surface potential variation on the nanopore ionic conductivity was performed in [41] and verified against a number of existing experimental datasets.

In this work, we perform a comprehensive theoretical and experimental study of ionic conductivity of a nanoporous membrane with electrically conductive surface. Unlike the previous works, we assume that the potential of membrane surface is not controlled externally, but the membrane is floating in the applied electric field. The 2D Space charge and 1D Uniform potential models are employed to describe the ion transport. The analytical solutions for ionic current and distributions of potential, ion concentrations, and pressure are derived for the first time assuming potential-dependent surface charge. It is shown that polarization of nanopore surface by the applied electric field leads to the enhancement of conductivity with increasing the transmembrane potential. The interaction between electronic and chemical surface charge is investigated. The theoretical predictions of conductivity enhancement are first confirmed by the experimental measurements in a porous anodic alumina membrane with carbon nanotubes inside the pores.

The paper is organized as follows. The theoretical models and solutions are presented in Section 2, while the membrane preparation and conductivity measurements are described in Section 3. The theoretical results are discussed and analyzed in Section 4 and the comparison with experiments is performed in Section 5.

2. Theoretical part

2.1. Problem statement

We consider a porous membrane of thickness L_p, which separates two reservoirs denoted by left (L) and right (R). An aqueous solution of monovalent and symmetric electrolyte with concentration C_0 is placed in the reservoirs, which are kept at equal pressures P_0 assumed to be zero for simplicity. The potential difference $\Delta\Phi = \Phi_R - \Phi_L$ between the reservoirs is applied. It results in the electric field, which causes the motion of ions through the membrane. The latter is idealized as an array of cylindrical nanopores with length L_p and radius R_p assuming that $L_p \gg R_p$. Thus, it is sufficient to consider the ion transport through a single nanopore. The two-dimensional nanopore geometry is described using the cylindrical coordinates R and Z in radial and axial directions, respectively, see Fig. 1a. The boundary layers of thickness L_b from both sides of the nanopore can be considered to account for concentration polarization if it is relevant.

The ionic conductivity G (S) of the nanopore is the ratio of ionic current I through it to the applied voltage U:

$$G = \frac{I}{U},$$

where $U = -\Delta\Phi = \Phi_L - \Phi_R$. The sign of ionic current is determined by the direction of electric field, so it is positive when the potential difference between left and right reservoirs is positive. The specific conductivity κ (S/m) of a cylindrical nanopore is defined by

$$\kappa = G\frac{L_p}{S_p}, \tag{1}$$

where $S_p = \pi R_p^2$ is the nanopore cross-sectional area.

The nanopore surface is assumed to be electrically conductive with electronic charge density Σ_e and electrical potential Φ_e, see Fig. 1b. The solution side of electric double layer (EDL) is divided into the Stern layer and the diffuse layer with relative permittivities ε_s and ε, electrical potentials $\Phi_s(R,Z)$ and $\Phi(R,Z)$, and thicknesses δ_s and $R_p - \delta_s$, respectively. The diffuse layer contains ions and water molecules, while only water molecules are present inside the Stern layer. The interface between these layers (oHp, the outer Helmholtz plane) has the potential $\Phi_d(Z)$. At the oHp, we assume the presence of chemical charge Σ_c, which may result from the adsorption of ions or dissociation of surface functional groups. Here Σ_c is considered to be constant. For a polarizable conductive nanopore wall floating in an external electric field, the total electronic charge is conserved and we assume it to be zero:

$$\int_0^{L_p}\int_0^{2\pi} \Sigma_e\, R_p\, d\Phi\, dZ = 0. \tag{2}$$

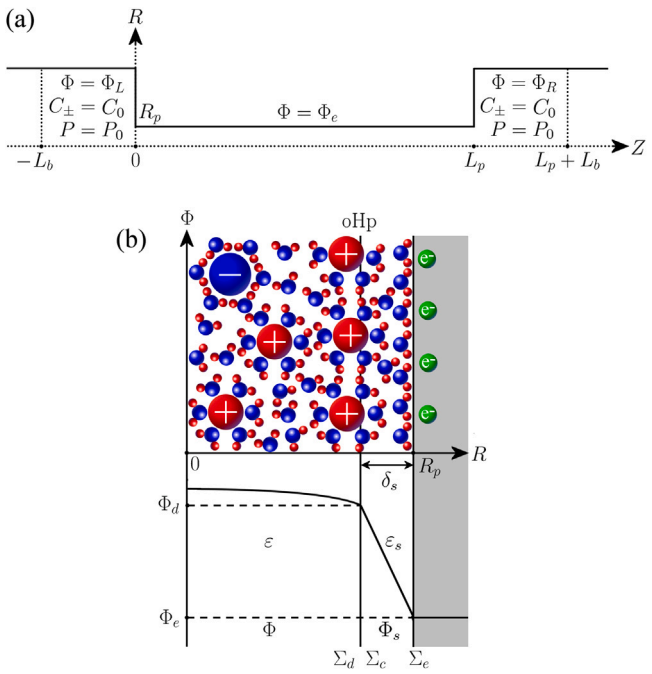

Fig. 1. The cylindrical nanopore (a) and the scheme of electric double layer (b).

The relation between charge density Σ_d at the oHp, the electronic charge density Σ_e at the nanopore wall, and chemical charge density Σ_c is derived from the boundary condition for electric fields at the oHp, see equation (S2) in Section 1 of the Supplementary Info. The result is written as [25,41]

$$\Sigma_d = \frac{R_p}{R_p - \delta_s}\Sigma_e + \Sigma_c = C_s\left(\Phi_e - \Phi_d\right) + \Sigma_c. \tag{3}$$

Here C_s is the Stern layer capacitance defined as

$$C_s = \frac{\varepsilon_s\varepsilon_0}{(R_p - \delta_s)\ln\left(\frac{R_p}{R_p-\delta_s}\right)},$$

where ε_0 is the vacuum permittivity.

To describe the ion transport in the diffuse layer, we consider the two-dimensional Space Charge (SC) model and one-dimensional Uniform Potential (UP) model. In these models, the assumption of point ions is employed. The calculations show that the variation of potential mostly occurs within the Stern layer (see Fig. 1), so no unphysical accumulation of ions at the diffuse layer boundary is expected. Thus, we do not take finite ion size effects [42,43] into account in this study. The description of SC and UP models in Sections 2.2 and 2.3 closely follows the works [25,41]. A novel model, which allows analytical solution for electrical potential, ion concentrations, pressure, and ionic current through the nanopore, is first proposed in this work on the basis of simplified UP model equations.

2.2. The Space Charge model of the diffuse layer

If the pore radius is larger than Debye length, then we have to take into account the radial variations of the electrical potential Φ, pressure P, cation C_+ and anion C_- concentrations, and solution velocity $\boldsymbol{U} = (U, V)$. The Space Charge model is based on the stationary Navier–Stokes, Nernst–Planck, and Poisson equations. This model was first suggested for the case of constant surface charge [15,21] and later extended to the case of constant surface potential [23].

The fluxes of ions induced by convection, diffusion, and electromigration are written as

$$\boldsymbol{J}_\pm = C_\pm\boldsymbol{U} - D_\pm\nabla C_\pm \mp \frac{D_\pm F}{R_g T}C_\pm\nabla\Phi,$$

where $D_\pm$ are the ion diffusion coefficients, R_g is the ideal gas constant, T is the temperature, and F is the Faraday constant. The dimensionless variables are introduced by

$$R = R_p' r, \qquad Z = L_p z, \qquad \boldsymbol{U} = \frac{D_-}{L_p}\boldsymbol{u}, \qquad P = C_* R_g T\, p,$$
$$C_\pm = C_* c_\pm, \qquad \Phi = \frac{R_g T}{F}\varphi, \qquad \boldsymbol{J}_\pm = \frac{D_- C_*}{L_p}\boldsymbol{j}_\pm. \tag{4}$$

Here $R_p' = R_p - \delta_s$, $\boldsymbol{u} = (u, v)$, and C_* is the reference concentration taken as $C_* = 1$ mol/m^3. The dimensionless potentials and surface charge densities on the pore wall and diffuse layer boundary are defined as follows

$$\Phi_e = \frac{R_g T}{F}\varphi_e, \quad \Phi_d = \frac{R_g T}{F}\varphi_d, \quad \Sigma_e = \frac{\varepsilon\varepsilon_0 R_g T}{F R_p}\sigma_e, \quad \Sigma_c = \frac{\varepsilon\varepsilon_0 R_g T}{F R_p'}\sigma_c,$$
$$\Sigma_d = \frac{\varepsilon\varepsilon_0 R_g T}{F R_p'}\sigma_d. \tag{5}$$

Let us introduce the quantities averaged over the diffuse layer. The dimensional average axial velocity is given by

$$\overline{V} = \frac{2}{R_p'^2}\int_0^{R_p'} V\, R\, dR. \tag{6}$$

The average pressure $\overline{P}$, ion concentrations $\overline{C}_\pm$, potential $\overline{\Phi}$, axial ion fluxes $\overline{J}_\pm$, total axial ion flux $\overline{J} = \overline{J}_+ + \overline{J}_-$, and axial charge flux $\overline{I} = \overline{J}_+ - \overline{J}_-$ are introduced in the same way. The corresponding dimensionless quantities are $\overline{v}$, $\overline{p}$, $\overline{c}_\pm$, $\overline{\varphi}$, $\overline{j}_\pm$, $\overline{j} = \overline{j}_+ + \overline{j}_-$, and $\overline{i} = \overline{j}_+ - \overline{j}_-$.

The specific conductivity (1) can be expressed in terms of dimensionless average charge flux and potential difference as

$$\kappa = \frac{D_- C_* F^2}{R_g T}\frac{\overline{i}}{\varphi_L - \varphi_R}, \tag{7}$$

while the dimensional axial ionic current is given by

$$I = \frac{D_- C_*}{L_p}F\pi R_p^2\,\overline{i}.$$

The dimensionless axial velocity, ion concentrations, and electrical potential in the SC model are sought in the form [21]:

$$\varphi(r,z) = \phi_v(z) + \psi(r,z), \quad c_\pm(r,z) = c_v(z)\exp(\mp\psi(r,z)), \tag{8}$$
$$p(r,z) = p_v(z) + 2c_v(z)\cosh(\psi(r,z)).$$

In this representation, the ion concentrations satisfy the Boltzmann distribution, and ϕ_v, c_v, p_v are the so–called virtual potential, concentration, and pressure. It follows from (S4), (4), (5), and (8) that

$$\varphi_d(z) = \phi_v(z) + \psi(1,z), \qquad \sigma_d(z) = \frac{\partial\psi}{\partial r}(1,z). \tag{9}$$

The dimensionless electronic charge is derived from (S3) taking into account solution (S1), boundary condition (S2), relations (S4), and definitions (5):

$$\sigma_e(z) = \sigma_d(z) - \sigma_c. \tag{10}$$

Eq. (10) is the dimensionless analogue of Eq. (3).

Function ψ is determined by solving the Poisson equation [25,41]

$$\frac{1}{r}\frac{\partial}{\partial r}\left(r\frac{\partial\psi(r,z)}{\partial r}\right) = \frac{c_v(z)}{\lambda^2}\sinh\psi(r,z) \tag{11}$$

with the condition of axial symmetry at $r = 0$:

$$\frac{\partial\psi}{\partial r}(0,z) = 0. \tag{12}$$

The boundary condition at the oHp ($r = 1$) is derived from (3) taking into account relations (4), (5), (8):

$$\psi(1,z) + \nu\frac{\partial\psi}{\partial r}(1,z) = \varphi_e - \phi_v(z) + \nu\sigma_c. \tag{13}$$

Here $\lambda = \sqrt{\varepsilon\varepsilon_0 R_g T/2F^2 C_*}/R_p'$ is the dimensionless Debye length, and $\nu = (\varepsilon/\varepsilon_s)\ln(R_p/R_p')$.

The conservation of total electronic charge given by Eq. (2) is expressed in dimensionless form with the help of (9) and (10) as follows

$$\int_0^1 \sigma_e(z)dz = \int_0^1 \frac{\partial \psi}{\partial r}(1,z)dz - \sigma_c = 0. \tag{14}$$

This is also known as floating boundary condition [23,26], from which the surface potential φ_e should be determined.

The average volume flux (or average axial velocity) $\overline{v}$, average ion flux $\overline{j}$, and average charge flux $\overline{i}$ are related to the gradients of virtual pressure p_v, virtual chemical potential $\mu_v = \ln c_v$, and virtual electrical potential ϕ_v by the symmetric 3×3 matrix $L = -\mathcal{L}^{-1}$ [21]:

$$\left(\frac{dp_v}{dz}, \frac{d\mu_v}{dz}, \frac{d\phi_v}{dz}\right)^T = L\left(\overline{v}, \overline{j}, \overline{i}\right)^T. \tag{15}$$

The coefficients of matrix $\mathcal{L} = \{\mathcal{L}_{ij}(z)\}$ depend on the function $\psi(r,z)$ and virtual concentration $c_v(z)$ and can be found in Section 2 of the Supplement Information.

The boundary conditions for Eqs. (15) are derived from (8) by substituting $\psi(r,z) = 0$ and taking into account the dimensional values of potential, ion concentration, and pressure in the reservoirs (see Section 2.1 and Fig. 1a):

$$\begin{aligned} z = 0: &\quad p_v = -2c_0, \quad c_v = c_0, \quad \phi_v = \varphi_L, \\ z = 1: &\quad p_v = -2c_0, \quad c_v = c_0, \quad \phi_v = \varphi_R. \end{aligned} \tag{16}$$

The detailed solution methodology is described in Section 3 of the Supplement Information.

2.3. The Uniform potential model of the diffuse layer

If the nanopore radius is comparable with or less than the Debye length, we can neglect the radial dependence of potential, ion concentrations, and pressure. In this case, the equations of SC model are significantly simplified and reduced to what is known as Uniform potential (UP) model. Then the potential $\Phi(Z)$ coincides with the potential Φ_d at the oHp, while ion concentrations $C_\pm(Z)$ and pressure $P(Z)$ depend only on the longitudinal coordinate Z.

Let us introduce the dimensionless electronic, chemical, and diffuse volume charge densities:

$$X_e = \frac{2\Sigma_e}{FR_pC_*}, \qquad X_c = \frac{2\Sigma_c}{FR_p'C_*}, \qquad X = \frac{2\Sigma_d}{FR_p'C_*}.$$

Eq. (3) can be rewritten as

$$X = \frac{R_p}{R_p'}X_e + X_c = c_s(\varphi_e - \varphi) + X_c, \tag{17}$$

where

$$c_s = \frac{2R_gC_sT}{F^2R_p'C_*}$$

is the dimensionless Stern layer capacitance.

The electroneutrality condition requires that X must be equal in magnitude and opposite in sign to the ionic charge density

$$X = c_- - c_+. \tag{18}$$

The UP model governing equations are derived from the SC model equations by ignoring the radial dependency of all variables. The elements of matrix L are simplified and Eqs. (15) are reduced to the system of three ordinary differential equations [25,41]:

$$\begin{aligned} \frac{dp}{dz} &= -8\alpha\overline{v} + X\frac{d\varphi}{dz}, \\ \frac{dc}{dz} &= \frac{1}{2cD}\Big((D+1)(c^2 - X^2)\overline{v} - ((D-1)X + (D+1)c)\,\overline{j} \\ &\qquad - ((D+1)X + (D-1)c)\,\overline{i}\Big) - \frac{c_sX}{c}\frac{d\varphi}{dz}, \\ \frac{d\varphi}{dz} &= \frac{1}{2D(c+c_s)}\Big(\big((D-1)c - (D+1)X\big)\overline{v} - (D-1)\overline{j} - (D+1)\overline{i}\Big). \end{aligned} \tag{19}$$

Here $c = c_+ + c_-$ is the total concentration of cations and anions, and $\alpha = \mu D_-(C_0R_gTR_p'^2)^{-1}$ is a parameter.

The boundary conditions inside the pore at the inlet from the left reservoir and at the outlet to the right reservoir are written as [25]:

$$z = 0: \qquad p = c - 2c_0, \quad c = \sqrt{X^2 + 4c_0^2}, \quad \varphi = \varphi_0, \tag{20}$$

$$z = 1: \qquad p = c - 2c_0, \quad c = \sqrt{X^2 + 4c_0^2}, \quad \varphi = \varphi_1. \tag{21}$$

These conditions describe the osmotic pressure jumps, concentrations jumps, and the Donnan potential jumps at the pore interfaces, respectively. Taking into account the concentration jumps $c_\pm = c_0\exp\left(\mp(\varphi_0 - \varphi_L)\right)$ at $z = 0$ and $c_\pm = c_0\exp\left(\mp(\varphi_1 - \varphi_R)\right)$ at $z = 1$ and combining them with Eqs. (17) and (18), we obtain the equations for determination of potentials φ_0 and φ_1:

$$c_s\left(\varphi_e - \varphi_0\right) + X_c = 2c_0\sinh\left(\varphi_0 - \varphi_L\right), \tag{22}$$

$$c_s\left(\varphi_e - \varphi_1\right) + X_c = 2c_0\sinh\left(\varphi_1 - \varphi_R\right). \tag{23}$$

The condition of total electronic charge conservation (2) is now expressed as

$$\int_0^1 c_s(\varphi_e - \varphi)dz = 0. \tag{24}$$

The algorithm for solving the UP model problem is described in Section 4 of the Supplement Information.

When concentration polarization is taken into account, one should solve the ion transport equations in two boundary layers of thickness L_b (see Fig. 1a). The corresponding equations and boundary conditions are presented in Section 5 of the Supplement Information.

2.4. Analytical model of ion transport in a polarizable nanopore

In this section, we derive an analytical solution of the UP model under a number of simplifying assumptions: the average velocity is zero ($\overline{v} = 0$), the chemical charge is absent ($X_c = 0$), and the ions have equal diffusion coefficients ($D = 1$). The first assumption means that the axial velocity depends on the radial coordinate in such a way that the fluid is moving in opposite directions in different parts of the nanopore cross-section (see formula (6)). At the same time, the total flow through any cross-section is absent. The validity of this assumption for the considered configuration will be confirmed by comparing the results with the 2D Space Charge model in Section 4.1. The second assumptions allows us to focus on the situation when only the electronic charge determines the conductive properties of the nanopore. Finally, the third assumption means that cations and anions equally contribute to the total ionic current in a neutral electrolyte. So, it is valid for electrolytes with close values of ion diffusion coefficients (such as aqueous KCl solution).

Under the proposed assumptions, Eqs. (19) are reduced to

$$\frac{dp}{dz} = c_s(\varphi_e - \varphi)\frac{d\varphi}{dz}, \tag{25}$$

$$\frac{dc}{dz} = -\overline{j} + c_s(\varphi_e - \varphi)\frac{d\varphi}{dz}, \tag{26}$$

$$\frac{d\varphi}{dz} = -\frac{\overline{i}}{c + c_s}. \tag{27}$$

They should be solved subject to boundary conditions (20), (21) and relation (24). It follows from (25) and (26) that

$$\frac{dc}{dz} = -\overline{j} + \frac{dp}{dz}.$$

Integration of this equation from $z = 0$ to variable z taking into account boundary conditions (20) gives $p = c - 2c_0 + \overline{j}z$. Applying boundary conditions (21) leads to $\overline{j} = 0$, thus

$$p = c - 2c_0. \tag{28}$$

Now let us integrate (26) subject to boundary conditions (20) at $z = 0$:

$$c = \frac{c_s}{2}\left((\varphi_e - \varphi_0)^2 - (\varphi_e - \varphi)^2\right) + \sqrt{c_s^2(\varphi_e - \varphi_0)^2 + 4c_0^2}. \quad (29)$$

Applying boundary conditions (21) at $z = 1$ results in the following relation

$$\sqrt{c_s^2(\varphi_e - \varphi_0)^2 + 4c_0^2} - \sqrt{c_s^2(\varphi_e - \varphi_1)^2 + 4c_0^2} + \frac{c_s}{2}\left((\varphi_e - \varphi_0)^2 - (\varphi_e - \varphi_1)^2\right) = 0. \quad (30)$$

At the next step, we express dz from (27) and substitute it into relation (24) taking into account (29):

$$\int_0^1 c_s(\varphi_e - \varphi)dz = -\int_{\varphi_0}^{\varphi_1} c_s(\varphi_e - \varphi)\frac{c + c_s}{\bar{i}}d\varphi = \quad (31)$$
$$= \frac{c_s}{2\bar{i}}(\varphi_1 - \varphi_0)(2\varphi_e - \varphi_0 - \varphi_1) \times \left(\frac{c_s}{4}(\varphi_1 - \varphi_0)(2\varphi_e - \varphi_0 - \varphi_1) + \sqrt{c_s^2(\varphi_e - \varphi_0)^2 + 4c_0^2} + 1\right) = 0.$$

Assuming that the applied potential difference is non-zero ($\varphi_L \neq \varphi_R$), we can easily see from (22) and (23) that $\varphi_1 \neq \varphi_0$. Thus, the only possibility to satisfy both relations (30) and (31) is $\varphi_e - \varphi_0 = \varphi_1 - \varphi_e$, i.e. the potential of the nanopore surface is the average between potentials just at the entrance and exit inside the nanopore:

$$\varphi_e = \frac{\varphi_0 + \varphi_1}{2}. \quad (32)$$

Let us now add (22) and (23), which gives

$$c_s(2\varphi_e - \varphi_0 - \varphi_1) = -4c_0 \sinh\left(\frac{\varphi_L + \varphi_R - \varphi_0 - \varphi_1}{2}\right) \times \cosh\left(\frac{\varphi_R - \varphi_L + \varphi_0 - \varphi_1}{2}\right).$$

As the left–hand side of this equation is zero due to (32), we find that $\varphi_L + \varphi_R = \varphi_0 + \varphi_1$, which leads to

$$\varphi_e = \frac{\varphi_L + \varphi_R}{2}. \quad (33)$$

Now we have rigorously proved that the nanopore surface potential is the arithmetic average of potentials specified at the left and right reservoirs. Only under this condition, the total electronic charge is zero and conserved when a potential difference is applied between the reservoirs. Similar conclusion was previously reported in [40] as a result of 2D numerical simulations. Note that the local electronic charge density can vary along the nanopore surface, which will be demonstrated in the next sections.

The expression for total ion concentration (29) can now be simplified using formula (32):

$$c = -\frac{c_s}{2}(\varphi - \varphi_1)(\varphi - \varphi_0) + \sqrt{c_s^2(\varphi_1 - \varphi_0)^2/4 + 4c_0^2}. \quad (34)$$

Let us now integrate Eq. (27), which leads to

$$\int_{\varphi_0}^{\varphi}(c + c_s)d\varphi' = -\bar{i}\int_0^z dz'.$$

Taking into account boundary conditions (20) and expression (34) for c, we find

$$(\varphi - \varphi_0)\left(\frac{c_s}{12}(\varphi - \varphi_0)(3\varphi_1 - 2\varphi - \varphi_0) + \sqrt{c_s^2(\varphi_1 - \varphi_0)^2/4 + 4c_0^2} + 1\right) = -\bar{i}z. \quad (35)$$

This equation implicitly determines the electrical potential φ as a function of coordinate z along the nanopore. Applying boundary conditions (21), we find the explicit formula for the charge flux

$$\bar{i} = -(\varphi_1 - \varphi_0)\left(\frac{c_s}{12}(\varphi_1 - \varphi_0)^2 + \sqrt{c_s^2(\varphi_1 - \varphi_0)^2/4 + 4c_0^2} + 1\right), \quad (36)$$

from which the ionic conductivity can be determined using formula (7). It follows from Eq. (27) and formula (36) that $\varphi(z)$ is a monotonically increasing (decreasing) function of z when $\varphi_1 > \varphi_0$ ($\varphi_1 < \varphi_0$), respectively. Thus, at fixed $z = z^*$ there is a single root $\varphi = \varphi^*$ of Eq. (35) at the interval $\varphi_0 < \varphi^* < \varphi_1$ ($\varphi_1 < \varphi^* < \varphi_0$), respectively. When $\varphi(z)$ is determined, one can calculate the total concentration from (34) and pressure from (28). Finally, the concentrations of cations and anions are given by $c_+ = (c - X)/2$ and $c_- = (c + X)/2$, respectively, where $X = c_s(\varphi_e - \varphi)$.

When the applied potential difference is small ($< RT/F$), Eqs. (22) and (23) can be solved using the approximate relation $\sinh x \approx x$. It gives

$$\varphi_1 - \varphi_0 = \frac{\varphi_R - \varphi_L}{1 + c_s/2c_0}.$$

The model developed in this section will be further referred to as UPS (Uniform Potential Simplified) model.

3. Experimental part

3.1. Preparation of PAA membranes

The porous anodic alumina (PAA) membranes were prepared according to the method previously described in [44]. The aluminum foil of high purity (99.999%) with the thickness of 500 μm was electrochemically polished in a solution of 1.85 M CrO_3 and 15.1 M H_3PO_4 at 80 °C in pulsed mode (40 pulses with 3 s duration of each pulse at current density of 0.5 A/cm^2 and 40 s interpulse interval). The anodization was performed in a 0.3 M sulfuric acid electrolyte in potentiostatic mode at 25 V and the temperature of 5 °C. The anodized area was a circle with the diameter of 40 mm on a 50 mm diameter aluminum foil. After the first anodization during 8 h, the alumina layer was removed in a solution of 0.2 M CrO_3 and 0.6 M H_3PO_4 at 60 °C during 40 min. The second anodization was performed under the same conditions during 15 h, which resulted in the membrane thickness of 70 μm. The aluminum substrate was selectively etched in the form of 11 mm diameter circles in a solution of 0.25 M $CuCl_2$ and 5 vol % HCl. Then the barrier layer was removed using a solution of 0.5 M H_3PO_4 with electrochemical detection of pore opening [45]. Membranes in the form of 10 mm diameter disks were obtained by cutting them from an aluminum frame with the help of laser (SharpMark–30SM Fiber smart, USA).

3.2. Carbon nanotube growth inside PAA membranes

The catalyst-free CVD was used to grow carbon nanotubes in the PAA membranes. The tube furnace OTF–1500X–UL–3 equipped with the liquid vaporization system LVD–F1 (MTI, USA) and the vacuum pump PC 3001 VARIO (Vacuubrand GMBH, Germany) was used. The ethanol (95.6%) – water (4.4%) mixture was employed as a carbon precursor. It was vaporized at 150 °C and mixed with argon gas by the vaporization system. A membrane sample was placed in the tube center using a quartz plate holder. The furnace was heated with the rate of 5 °C/min in an argon atmosphere at flow rate of 100 mL/min and pressure of 0.1 bar. The deposition was performed at temperature 750 °C and pressure of 0.5 bar during 180 min with ethanol–water flow rate 0.083 ml/min in the liquid phase and argon flow rate 200 ml/min. Then the sample was cooled to 150 °C with the rate of 5 °C/min in an argon atmosphere. The membranes with carbon nanotubes will be further referred to as C–PAA membranes.

3.3. Membrane characterization

The morphology of membranes was characterized by the Scanning electron microscopy using FE–SEM Hitachi S–5500 instrument (Japan)

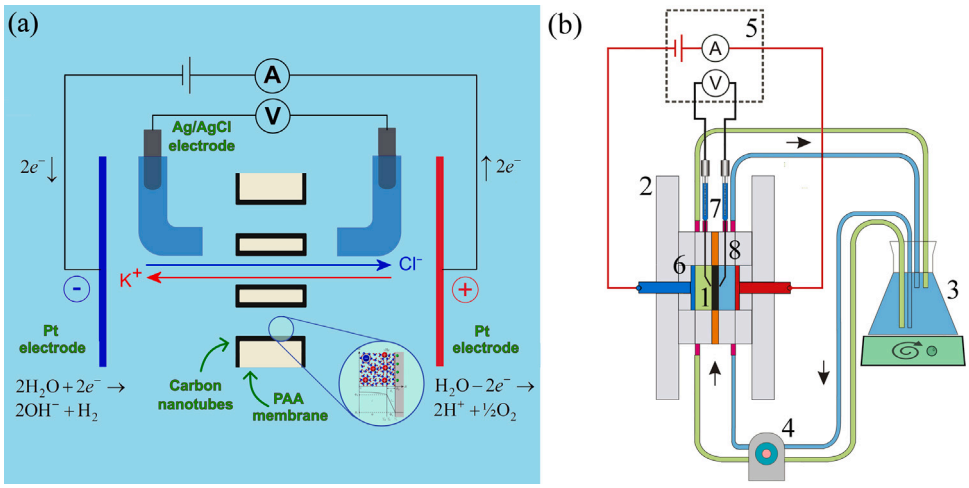

Fig. 2. The scheme of ionic current measurement (a) and the electrochemical cell (b).

operating at 5 kV. Before examination, the membrane samples were glued to a support and coated with platinum by magnetron sputtering (Emitech K575X DX, Quorum Technologies Ltd, Great Britain) during 1 min at the current of 10 mA and the pressure of $8 \cdot 10^{-6}$ Bar in argon atmosphere. The samples of membrane cross-sections for TEM studies were prepared by focused ion beam system Hitachi FB–2100 (Japan) operating at 40 kV with additional 1 kV Ar+ ion polishing by Leica RES 102 (Austria). The TEM images were obtained by Hitachi HT7700 (Japan) at 100 kV accelerating voltage. The pore size distribution of prepared membranes was determined by processing of SEM and TEM images using the methodology described in details in [44].

3.4. Measurement of ionic current

To study the ionic conductivity of PAA membranes, a special electrochemical cell was developed (Fig. 2). A membrane sample (1) was glued in the holder using epoxy resin and placed between two compartments of the cell (2) made of plexiglass. The area available for ion transport (19.6 mm^2) corresponded to a circle with the diameter of 5 mm. The cell parts were fixed together with screws and nuts. Milli–Q water (18 $M\Omega\,cm^{-1}$) was used to prepare working solutions and to wash the cell before each experiment. The solutions were also degassed to prevent bubbles nucleation. After assembling the cell, the compartments were filled with KCl aqueous solution of specified concentration from the 2 L flask (3) using peristaltic pump (4). During measurements, the solutions were pumped through the cell with the flow rate of 10–30 ml/min to avoid concentration polarization, especially at low salt concentrations [46–48].

Electrical measurements were performed using Potentiostat PI—50 Pro (Electrochemical instruments, Russia) in galvanostatic mode. The specified current was applied by the potentiostat (5) connected to platinum plates (6) with the size of 20 × 20 mm. The resulting voltage difference was measured using 4.2 M Ag/AgCl electrodes (7) connected to Luggin capillaries (8), which nozzles were located at a distance of 3 mm from the membrane. The measurements were performed until the stationary potential difference was established (typically 10–100 s depending on salt concentration). The transmembrane voltage was determined by subtracting the voltage difference measured in the cell with membrane from that measured in the cell without membrane. The measurements were carried out in the range of KCl concentrations from 0.1 mM to 1 M (with a step of one order-of-magnitude) and in the range of applied currents from ±2 μA to ±10 mA, respectively (see more details in Section 5.2).

It should be noted that the stationary ion current through membrane pores was accompanied by water splitting with the evolution of hydrogen and oxygen at the cathode and anode, respectively (see Fig. 2a). As a result, the solution at the cathode (anode) space became more basic (acidic). The solutions were neutralized in the flask (3), which was put on a magnetic stirrer (see Fig. 2b). The change of electrolyte composition in the half–cells was negligibly small due to low currents, short measurement time, and pumping the solution from the flask of large volume (2 L). The situation shown in Fig. 2a corresponds to the case when the fluxes of K^+ and Cl^- are equal in magnitude and opposite in sign (see analytical model in Section 2.4). However, in the presence of chemical charge, the ion fluxes could be different due to selectivity of nanopore to cation or anion.

Assuming that a C–PAA membrane has straight cylindrical nanopores, the specific conductivity of a nanopore can be calculated from the measured current I under applied voltage difference U according to the formula

$$\kappa = \frac{I}{U}\frac{L_p}{\epsilon S}. \tag{37}$$

Here S is the membrane area and ϵ is the C–PAA membrane porosity calculated as

$$\epsilon = \frac{\pi}{2\sqrt{3}}\left(\frac{D_p}{D_{ip}}\right)^2, \tag{38}$$

where D_p is the pore diameter and D_{ip} is the distance between centers of neighboring pores [44].

4. Results and discussion

4.1. The impact of polarization on the ion transport in a single nanopore

We start from theoretical description of ion transport in a single nanopore with the help of SC and UP models. The pore length $L_p = 70$ μm corresponds to the porous anodic alumina membranes synthesized in this work, while the pore radius is taken as $R_p = 8$ nm. It is assumed that the potentials in the reservoirs are set to $P_L = -\Delta\Phi/2$ and $P_R = +\Delta\Phi/2$, where $\Delta\Phi$ is the applied potential difference. The Stern layer thickness is taken as $\delta_s = 0.5$ nm and the Stern layer capacitance is $C_s = 0.1$ F/m^2. The calculations are performed for aqueous KCl solution with diffusion coefficients $D_+ = 1.957 \cdot 10^{-9}$ m^2/s for K^+ ion and $D_- = 2.032 \cdot 10^{-9}$ m^2/s for Cl^- ion. The dynamic viscosity is taken as $\mu = 0.888 \cdot 10^{-3}$ Pa s. The chemical charge is absent ($\Sigma_c = 0$).

The typical profiles of potential, ion concentrations, pressure, and electronic surface charge density in a conductive polarizable nanopore are shown in Fig. 3. It can be seen that the electric field inside the nanopore (Fig. 3a) induces a non-uniform electronic charge distribution on the conductive surface (Fig. 3d) while keeping the total surface charge zero. In other words, the surface is polarized by the electric field.

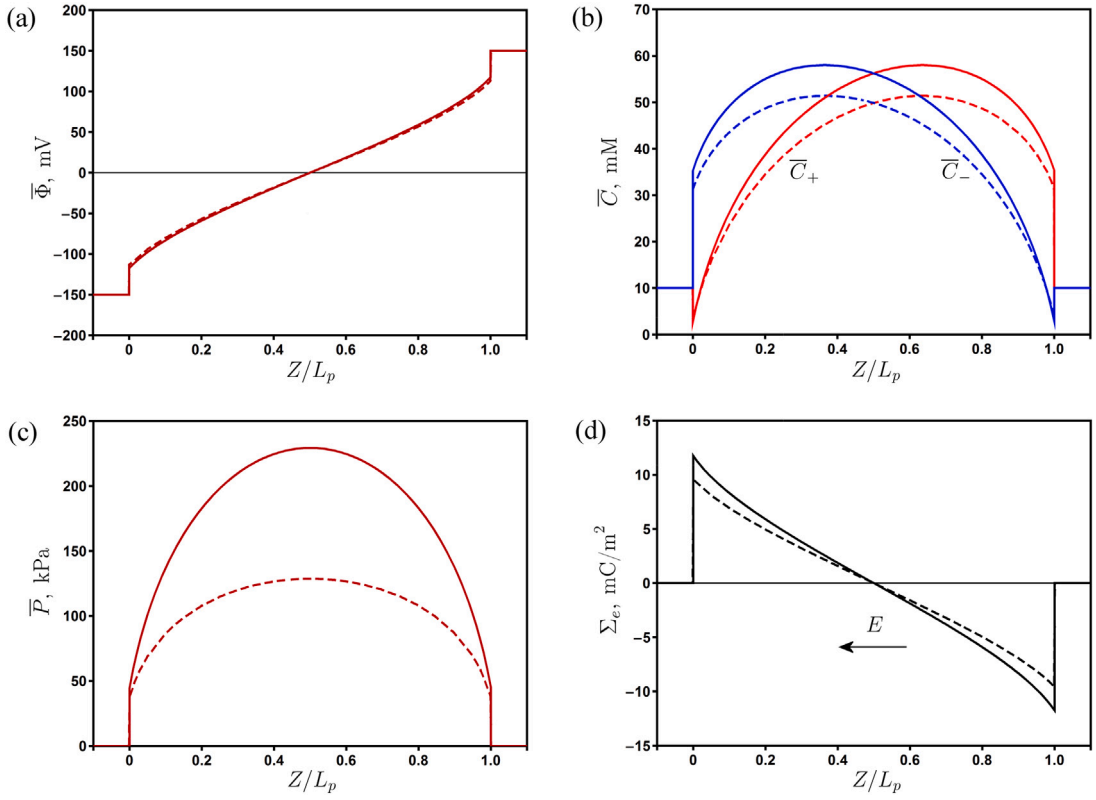

Fig. 3. The average potential (a), ion concentrations (b), pressure (c), and surface charge density (d) calculated from SC model (dashed curves) and from UP model (solid curves). $R_p = 8$ nm, $L_p = 70$ μm, $C_0 = 10$ mM, $C_s = 0.1$ F/m^2, $\Delta\Phi = 300$ mV.

It leads to the increase of anion (cation) concentration in the left (right) part of the nanopore (Fig. 3b), where the surface charge is positive (negative). As a result, the concentration of ions (charge carriers) inside the nanopore increases in comparison with that in the reservoirs. It leads to the enhancement of nanopore ionic conductivity ($\kappa = 0.5567$ S/m) in comparison with conductivity of 10 mM KCl bulk solution ($\kappa = 0.1498$ S/m). The pressure is symmetric with respect to the center of the pore and reaches maximum at that point (Fig. 3c). It results from the specific structure of electroosmotic flows in the nanopore (to be discussed below).

Note that the cross-sectionally averaged profiles of potential and ion concentrations as well as electronic charge density obtained from the SC model are rather close to those obtained from the UP model. However, the latter overestimates the pressure magnitude by almost two times in comparison with the former. As for the UPS model derived in Section 2.4, its predictions fully coincide with numerical results based on the UP model.

The results of two-dimensional calculations are presented in Fig. 4. The potential slightly varies with radial coordinate and increases (decreases) towards the wall when $0 < Z/L_p < 0.5$ ($0.5 < Z/L_p < 1.0$), see Fig. 4a. The surface potential Φ_e is zero as expected from formula (33) since the potentials in the reservoirs are equal in magnitude and opposite in sign. There is a strong potential change within the Stern layer, which is shown by darker areas near the nanopore walls. The ion concentration fields demonstrate a complex shape (Fig. 4b) with cation (anion) concentration increasing towards the wall in the negatively (positively) charged part of the nanopore. The electric field interacts with the excess of negative (positive) charge near the walls in the corresponding part of the nanopore $0 < Z/L_p < 0.5$ ($0.5 < Z/L_p < 1.0$). It results in the electroosmotic flows near the walls towards the nanopore entrance ($Z = 0$) and exit ($Z = L_p$) and in opposite direction in the central part of the nanopore (Fig. 4d). These flows compensate each other in such a way that the total flow through the nanopore remains zero ($\overline{V} = 0$, see formula (6)). In addition, they result in the pressure distribution, which is symmetric with respect to the nanopore center ($Z/L_p = 0.5$) and reaches maximum at that point (Fig. 4c). Note that the 2D calculations show that the assumption of zero average axial velocity is justified when deriving the analytical UPS model in Section 2.4.

4.2. The salt concentration effect on conductivity enhancement

Now let us investigate the impact of salt concentration on the enhancement of ionic current and conductivity by the polarization effect. The results of calculations are shown in Fig. 5. For convenience, the ionic current is normalized to its absolute value I_{max} at $\Delta\Phi = 500$ mV.

When the applied potential difference is close to zero, the induced charge is very small, so the nanopore specific conductivity coincides with that of bulk solution of a given salt concentration (Fig. 5a). The rise of potential difference increases the induced charge, which leads to the increase of ion concentrations inside the nanopore (Fig. 3b) and the corresponding enhancement of conductivity. This effect is most pronounced at low concentrations, where the enhancement can reach a few orders of magnitude. In this case, the current–voltage curves show strong non-linearity, see Fig. 5b. At larger salt concentrations, the relative change of ion concentrations inside the nanopore due to polarization effect becomes smaller, so the conductivity enhancement with the rise of applied potential difference gets lower. In this case, the current–voltage curves tend to linear form. It should be noted that the UP and UPS models show practically the same results. Analytical formula (36) for the charge flux can explain the observed variation of conductivity enhancement with salt concentration. It results from the relative importance of electronic charge contribution (terms proportional to $c_s(\varphi_1 - \varphi_0)$) and salt concentration contribution (term c_0^2) to the ionic current.

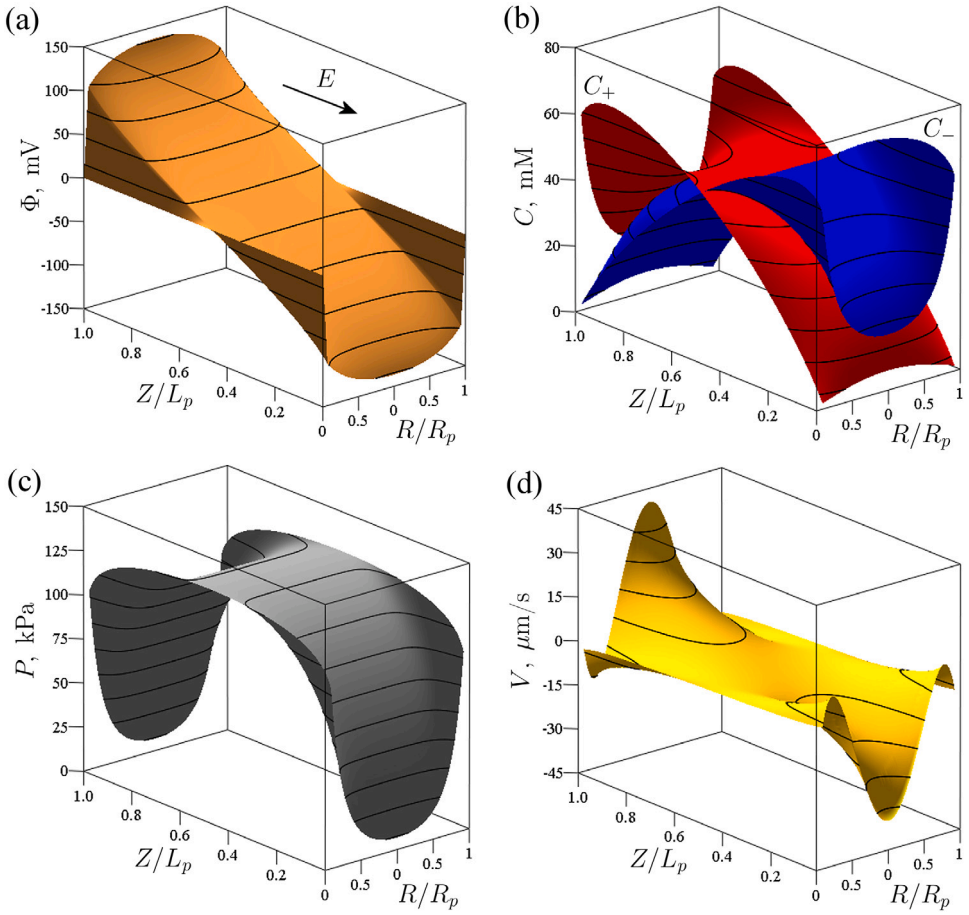

Fig. 4. The fields of potential (a), ion concentrations (b), pressure (c), and axial velocity (d) calculated from 2D SC model. $R_p = 8$ nm, $L_p = 70$ μm, $C_0 = 10$ mM, $C_s = 0.1$ F/m^2, $\Delta\Phi = 300$ mV.

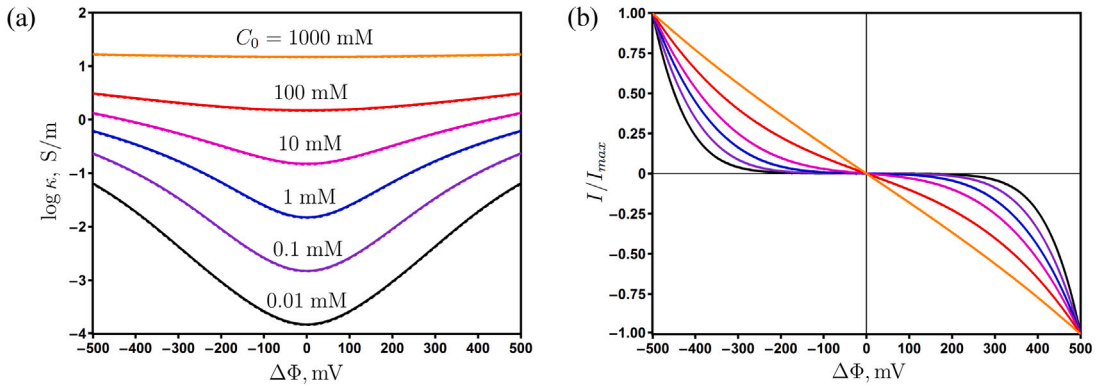

Fig. 5. The dependence of specific conductivity (a) and normalized ionic current (b) on the applied potential difference for different KCl concentrations based on the UP model (solid curves) and the UPS model (dashed curves). The solid and dashed curves almost coincide. $R_p = 8$ nm, $L_p = 70$ μm, $C_s = 0.1$ F/m^2.

4.3. The Stern layer capacitance effect on conductivity enhancement

Fig. 6a shows the impact of Stern layer capacitance C_s on the specific conductivity of the nanopore. As the induced electronic charge is proportional to C_s (see formulas (3) and (17)), the enhancement of ionic conductivity with increasing the applied potential difference is stronger for larger C_s. The non-linearity of current–voltage curves becomes more pronounced with increasing C_s, see Fig. 6b. The agreement between the UP and UPS models is perfect. The contribution of induced electronic charge to the ionic current and conductivity is determined by two terms proportional to c_s in formula (36).

4.4. The effect of chemical charge density on conductivity enhancement

In this section, we analyze how the presence of chemical charge at the oHp can affect the ionic conductivity of the nanopore. Fig. 7a shows the dependence of specific conductivity on the applied potential difference ΔΦ. In the absence of chemical charge, the conductivity tends to its minimum when ΔΦ tends to zero. The increase of potential difference enhances the nanopore conductivity due to increase of ions concentration, which is caused by the induced electronic charge, see Section 4.1. In this case, the current–voltage curve is strongly non-linear (Fig. 7b). When the chemical charge density Σ_c becomes non-zero, we first observe the increase of conductivity at small potential

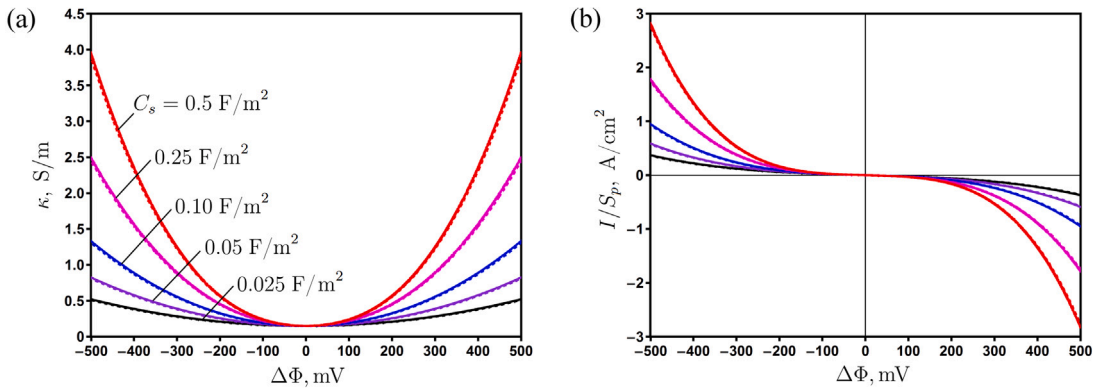

Fig. 6. The dependence of specific conductivity (a) and ionic current density (b) on the applied potential difference for different Stern layer capacitances based on the UP model (solid curves) and the UPS model (dashed curves). The solid and dashed curves almost coincide. $R_p = 8$ nm, $L_p = 70$ μm, $C_0 = 10$ mM.

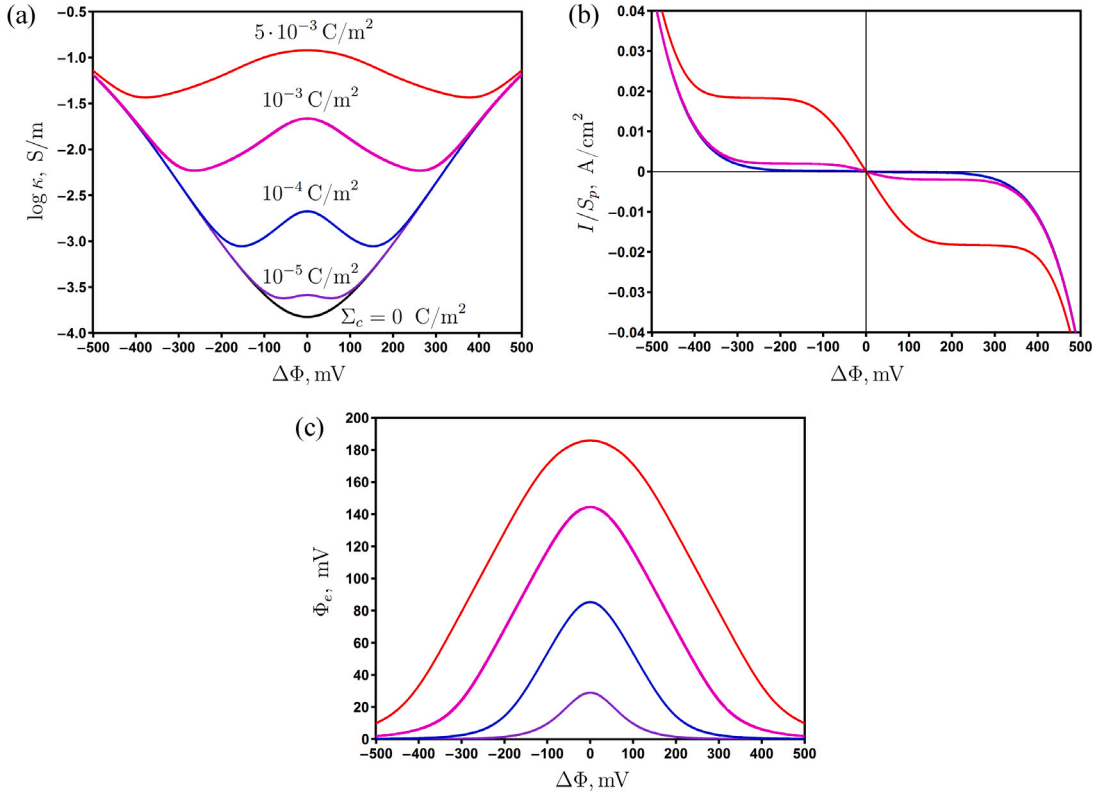

Fig. 7. The dependence of specific conductivity (a), ionic current density (b), and surface potential (c) on the applied potential difference for different values of chemical charge density based on the UP model. $R_p = 8$ nm, $L_p = 70$ μm, $C_s = 0.1$ F/m^2, $C_0 = 0.01$ mM.

differences. In this region, the contribution of induced charge is small, so the conductivity is controlled by the chemical charge. When the latter increases, there appears a linear region on the current–voltage curve. When $\Delta\Phi$ tends to zero, the conductivity attains its local maximum, while two local minima are observed at two values of $\Delta\Phi$, which are equal in magnitude and opposite in sign. In this region, the chemical charge is partially screened by the induced electronic charge. In the two ranges of $\Delta\Phi$ values between local maximum and two local minima, the ionic current becomes independent on the applied potential difference, see Fig. 7b. When the magnitude of $\Delta\Phi$ is increased further, the conductivity follows the curve corresponding to $\Sigma_c = 0$. In this region, the contribution of induced electronic charge is much larger than that of chemical charge.

The dependence of surface potential on the applied potential difference is shown in Fig. 7c. Note that in the absence of chemical charge, the requirement of zero total electronic charge requires the surface potential to be zero. The increase of chemical charge leads to the rise of surface potential at small $\Delta\Phi$. In this case, the chemical charge is dominant and it determines the value of Φ_e. However, with increasing the magnitude of $\Delta\Phi$, the induced electronic charge becomes dominant with one half of the pore being negatively charged and the other half being positively charged, so the surface potential tends to zero to ensure the conservation of electronic charge.

Finally, we would like to note that the conductivity dependence on the applied voltage difference is symmetric with respect to $\Delta\Phi = 0$ (see Figs. 5–7). It is related to the fact that the nanopore surface is polarized by the external electric field in such a way that the electronic charge in one half of the pore is positive, while in the other half it is negative. It is demonstrated in Figs. 3 and 4. So, when the applied potential difference changes its sign to the opposite one, these halves are exchanged, but the values of ionic current and conductivity remain the same. The calculations show that the presence of chemical charge does not

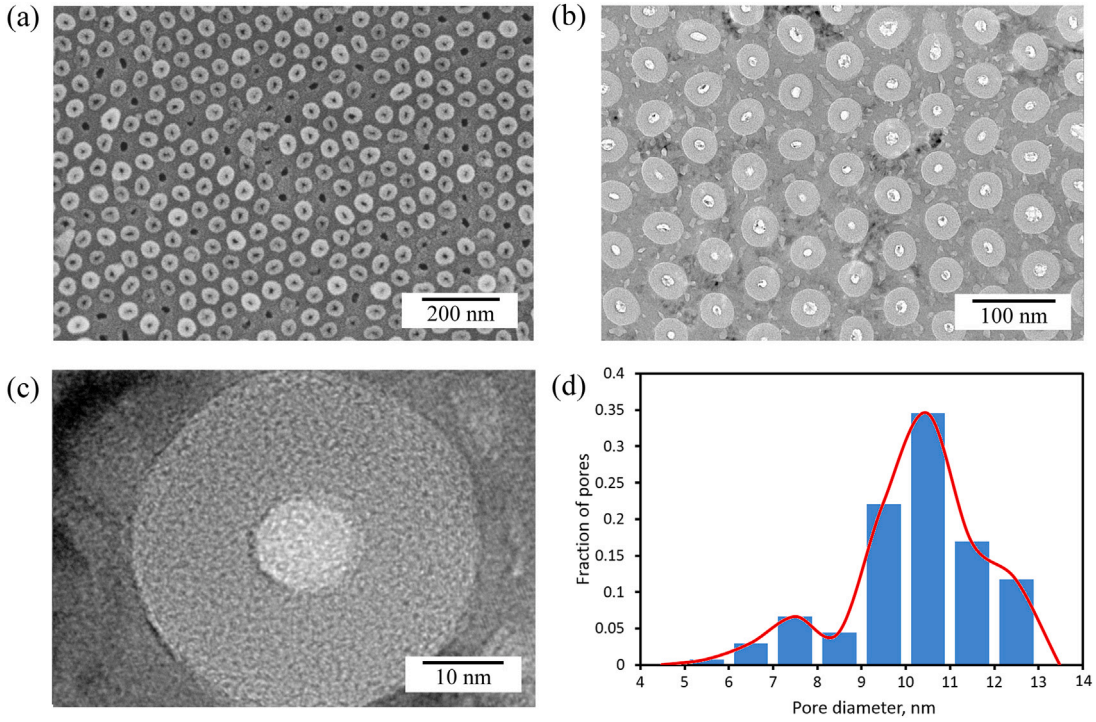

Fig. 8. SEM image (a) and TEM image (b) of membrane cross-section, TEM image of a single nanopore (c), and pore size distribution obtained by processing of TEM images (d).

affect this symmetrical behavior. It is characteristic for the considered system in contrast to the other systems such as e.g. nanofluidic ionic diodes, where the current and conductivity magnitudes change when the opposite potential difference is applied [37].

5. Ionic conductivity of porous anodic alumina membranes with carbon nanotubes

5.1. Membrane morphology

Let us now proceed to the experimental studies of ion transport through porous anodic alumina membranes with carbon nanotubes. The membrane morphology is presented in Fig. 8a. The SEM image shows a random horizontal cut of membrane, where some nanotubes stick out of the surface, while the other ones are hidden inside the membrane pores. The TEM image of membrane slice prepared by the FIB displays a regular structure of carbon nanotubes, which are embedded in all membrane pores (Fig. 8b). A single nanotube is shown in Fig. 8c. It can be seen that the nanotube wall consists of concentric layers of carbon.

The pore size distribution obtained by processing the TEM images is presented in Fig. 8d. The TEM data provide the pore diameter of 10.4 ± 1.5 nm. In the model calculations below, we assume that the pore diameter is $D_p = 10$ nm. The interpore distance is $D_{ip} = 65$ nm, so the membrane porosity calculated from formula (38) is $\epsilon = 0.0215$.

5.2. Current–voltage curves and ionic conductivity

In this section, we present the experimental results on conductivity measurement and compare them with model predictions. The 1D UP model is used with the parameters described in Section 4.1 except the Stern layer permittivity, which is taken as $C_s = 0.05$ F/m^2. This parameter controls the conductivity enhancement with variation of potential difference, so it is chosen lower to fit the experimental data.

The conductivity was measured in galvanostatic mode by applying constant current in the ranges ±2 μA, ±20 μA, ±200 μA, ±1.2 mA, ±10 mA for KCl concentrations 0.1 mM, 1 mM, 10 mM, 100 mM, 1000 mM, respectively. First, the potential drop in the cell without membrane was measured. At the highest current applied, it was 80–90 mV for 0.1 mM, 1 mM, 10 mM KCl solutions, and 40–50 mV for 100 and 1000 mM KCl solutions. This potential drop was subtracted from that measured in the cell with a C–PAA membrane. The latter was around 300–600 mV at the highest current applied.

We have found some difficulties in comparing the absolute values of ionic current I and specific conductivity κ calculated from the model using formula (1) and determined from experimental measurements using formula (37). The experimental values were 5–10 times smaller than the theoretical ones depending on the measured sample and salt concentration (see discussion below). It could be explained by the hypothesis that a part of nanopores might not be fully available for ion transport due to narrowing of pore diameter just near the membrane surface. To perform a meaningful comparison between experiment and theory, we normalize the experimental and calculated currents by their maximum values I_{max}. The calculated conductivity is normalized by its value when $\Delta\Phi \rightarrow 0$, while the experimental conductivity is normalized by κ_0, the average of conductivities measured at two lowest (negative and positive) currents. The experimental dependence of normalized conductivity is approximated by the model dependence using the chemical charge density as a fitting parameter.

The results are presented in Fig. 9. At KCl concentration of 1000 mM (Fig. 9a,b), the current–voltage curve is linear, and the conductivity is constant. When the concentration is decreased to 100 mM, the polarization effect starts to play a role. There is a slight enhancement of conductivity with the rise of potential difference, which leads to some non-linearity of current–voltage curve (Fig. 9c,d). In the case of 10 mM solution, these trends become much stronger (Fig. 9e,f). The conductivity is enhanced by around 4.6 times at $\Delta\Phi = \pm 440$ mV in comparison with k_0. At lower concentrations of 1 mM and 0.1 mM, the charge distribution induced on the nanopore walls leads to a significant increase of ion concentrations inside the nanopore. It leads to a significant rise of conductivity with $\Delta\Phi$ and strong non-linearity of current–voltage curve, see Fig. 9g,h and i,j. The values of chemical charge density, which were obtained by fitting the conductivity curves, are as follows: $\Sigma_c = 2.1 \cdot 10^{-4}$ C/m^2 for $C_0 = 0.1$ mM, $\Sigma_c = 1.3 \cdot 10^{-3}$ C/m^2

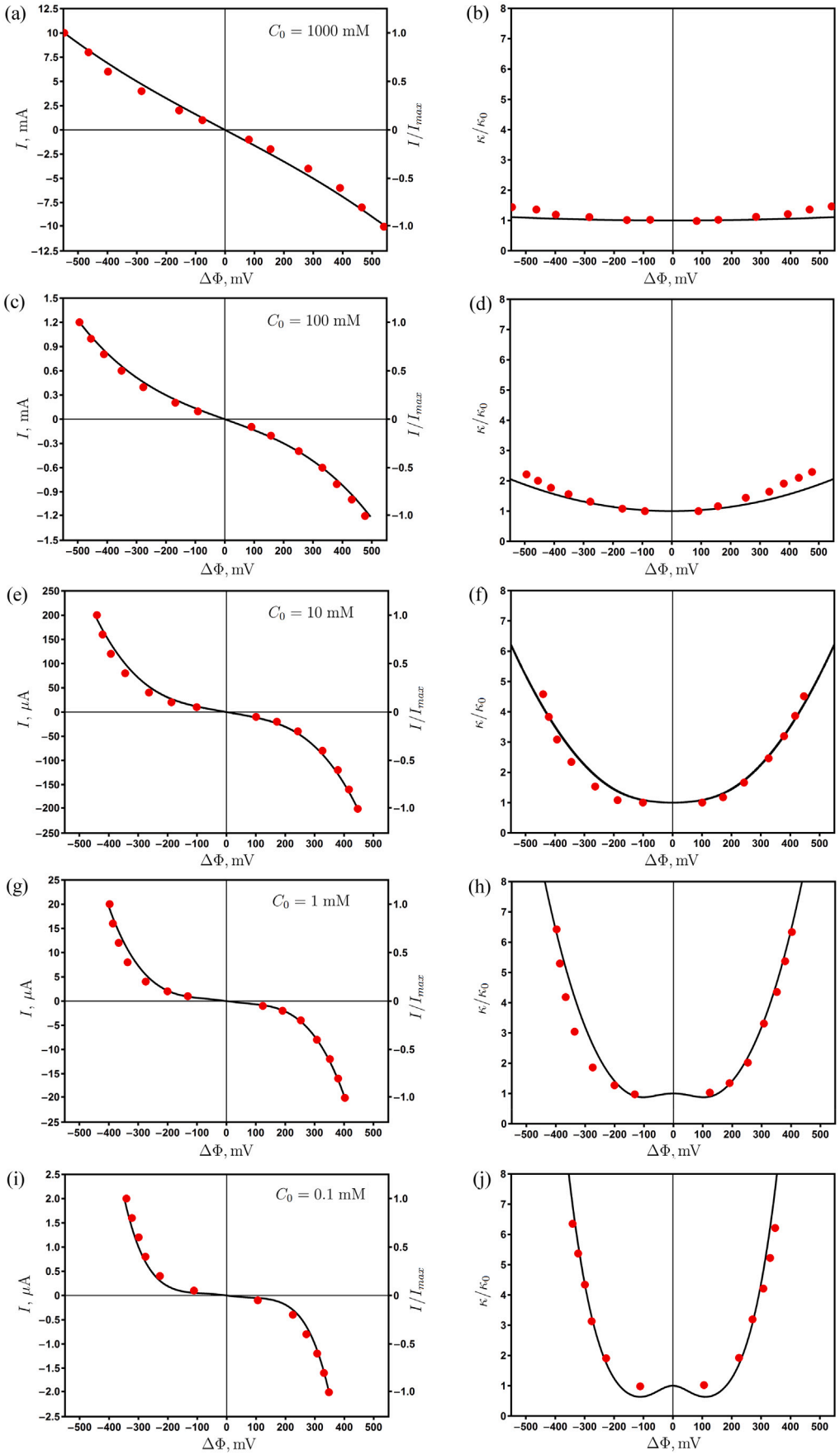

Fig. 9. The dependence of ionic current and normalized ionic conductivity on the applied potential difference for different KCl concentrations. Experiment (red circles) and 1D UP model calculations (black curves). The left axis in figures a,c,e,g,i corresponds to the experimental current values, while the right axis shows the calculated normalized current.

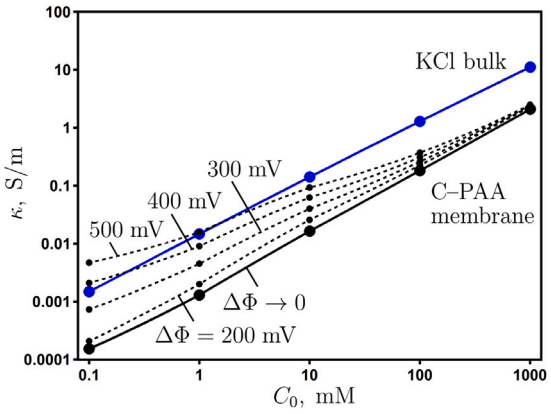

Fig. 10. The dependence of specific ionic conductivity on the KCl concentration. Bulk KCl aqueous solution (blue line), C–PAA membrane for different applied voltages (black dashed curves).

for $C_0 = 1$ mM, and $\Sigma_c = 4.3 \cdot 10^{-3}$ C/m^2 for $C_0 = 10$ mM. The increase of chemical charge density with the rise of salt concentration can be explained by adsorption of ions on the membrane surface. However, we cannot determine the sign of adsorbed charge from the measured conductivity data. Note that at higher concentrations (100 mM and 1000 mM), the variation of chemical charge does not affect the normalized conductivity as it turns to unity. Thus, for these concentrations we used the same Σ_c as for 10 mM. In general, we observe a remarkable agreement between experimental data and model calculations.

Fig. 10 shows the comparison between specific conductivity of bulk KCl aqueous solution (blue curve) and the experimentally measured specific conductivity of the same solution in the pores of C–PAA membrane (solid black curve) depending on salt concentration and voltage difference. One can see that at lowest voltages (lowest applied currents), the conductivity of C–PAA membrane is lower by one order of magnitude in comparison with that of bulk KCl. Nevertheless, both curves are almost parallel showing the same trend with increasing salt concentration. The dashed curves correspond to different applied voltages and are obtained from model predictions based on fitting the experimental data (see Fig. 9). The conductivity enhancement is negligible at high concentrations, but becomes stronger with decreasing salt concentration and reaches 28.2 times at $C_0 = 0.1$ mM and $\Delta\Phi = 500$ mV.

6. Conclusion

In this work, we have investigated the ionic conductivity of electrically conductive membranes. The 2D Space charge and 1D Uniform potential models are employed to describe the ion transport through a cylindrical nanopore with conductive surface. The latter separates two reservoirs with equal salt concentrations and pressures, but different electrical potentials. The models assume that the nanopore interior consists of a Stern layer and a diffuse layer with chemical charge present on the boundary between them.

The calculations show that the imposed electric field polarizes the conductive nanopore surface leading to redistribution of electrons on it. It leads to the continuous variation of electronic charge from positive to negative along the nanopore surface. At the same time, the total electronic charge is conserved and remains zero. A higher concentration of cations (anions) is observed at negatively (positively) charged part of the nanopore. The increase of charge carries concentration inside the nanopore due to polarization effect results in the enhancement of ionic conductivity with increasing the applied voltage difference. This enhancement can reach a few orders of magnitude at low salt concentrations, but becomes much smaller at high concentrations. It leads to the non-linear current–voltage curves. The conductivity enhancement is controlled by the electronic charge, which is proportional to the Stern layer capacitance. The presence of chemical charge has a screening effect on the interaction of electric field with the electronic charge on the nanopore surface, and reduces the enhancement of conductivity with increasing the applied voltage difference.

We have derived a novel analytical solution of 1D Uniform potential model for the charge flux and ionic conductivity assuming equal ion diffusion coefficients, zero average electroosmotic velocity, and the absence of chemical charge. It is shown that the conservation of electronic charge requires that the nanopore surface potential is the average between potentials imposed in the reservoirs separated by the nanopore. The analytical results are in perfect agreement with those provided by the full 1D UP model.

To verify the theoretical predictions, we have synthesized porous anodic alumina membranes and deposited carbon nanotubes inside the pores by chemical vapor deposition from ethanol precursor. It allows to obtain the matrix of straight cylindrical nanopores with electrically conductive surface and precisely controlled internal diameter. The ionic conductivity of obtained membranes is measured in KCl aqueous solution in the range of concentrations from 0.1 mM to 1000 mM. The experimental data are approximated by the 1D UP model curves using chemical charge as a fitting parameter. Strong enhancement of ionic conductivity (more than 6 times) and the corresponding non-linear dependence of current on the applied voltage is observed experimentally at low concentrations when the potential difference increases. The enhancement is reduced at large concentrations in agreement with theoretical predictions.

CRediT authorship contribution statement

Ivan A. Kharchenko: Investigation, Formal analysis, Data curation. **Nikita V. Vaulin:** Visualization, Methodology, Investigation. **Mikhail M. Simunin:** Methodology, Investigation, Formal analysis. **Semen A. Mareev:** Methodology. **Ivan V. Nemtsev:** Visualization, Investigation. **Alexandr S. Goltaev:** Investigation, Visualization. **Denis V. Lebedev:** Visualization, Methodology, Investigation, Formal analysis. **Ilya I. Ryzhkov:** Writing – review & editing, Writing – original draft, Visualization, Supervision, Software, Project administration, Methodology, Investigation, Funding acquisition, Conceptualization.

Declaration of competing interest

No conflict of interest is declared.

Data availability

Data will be made available on request.

Acknowledgments

This work is supported by the Russian Science Foundation, Project 23–19–00269. The physicochemical analysis of materials was carried out in Krasnoyarsk Regional Center of Research Equipment of Federal Research Center ‘Krasnoyarsk Science Center SB RAS’.

Appendix A. Supplementary data

Supplementary material related to this article can be found online at https://doi.org/10.1016/j.electacta.2024.144994.

References

[1] L.Y. Chu, Smart Membrane Materials and Systems, Springer–Verlag, Berlin, 2011.
[2] D. Wandera, S.R. Wickramasinghe, S.M. Husson, Stimuli-responsive membranes, J. Membr. Sci. 357 (2010) 6–35.
[3] X. Hou, W. Guo, L. Jiang, Biomimetic smart nanopores and nanochannels, Chem. Soc. Rev. 40 (2011) 2385–2401.
[4] Z. Zhang, G. Huang, Y. Li, X. Che, Y. Yao, S. Ren, M. Li, Y. Wu, C. An, Electrically conductive inorganic membranes: A review on principles, characteristics and applications, Chem. Eng. J. 427 (2022) 131987.
[5] A.B. Alayande, K. Goh, M. Son, C.M. Kim, K.J. Chae, Y. Kang, J. Jang, I.S. Kim, E. Yang, Recent progress in one– and two–dimensional nanomaterial–based electro–responsive membranes: Versatile and smart applications from fouling mitigation to tuning mass transport, Membranes 11 (2021) 5.
[6] M.J. Larocque, A. Gelb, D.R. Latulippe, C.F. Lannoy, Meta–analysis of electrically conductive membranes: A comparative review of their materials, applications, and performance, Sep. Purif. Technol. 287 (2022) 120482.
[7] M. Nishizawa, V.P. Menon, C.R. Martin, Metal nanotubule membranes with electrochemically switchable ion–transport selectivity, Science 268 (1995) 700–702.
[8] C.R. Martin, M. Nishizawa, K. Jirage, M. Kang, S.B. Lee, Controlling ion–transport selectivity in gold nanotubule membranes, Adv. Mater. 13 (2001) 1351–1362.
[9] M.S. Kang, C.R. Martin, Investigations of potential–dependent fluxes of ionic permeates in gold nanotubule membranes prepared via the template method, Langmuir 17 (2001) 2753–2759.
[10] S.P. Surwade, S.H. Chai, J.P. Choi, X. Wang, J.S. Lee, I.V. Vlassiouk, S.M. Mahurin, S. Dai, Electrochemical control of ion transport through a mesoporous carbon membrane, Langmuir 30 (2014) 3606–3611.
[11] H. Zhang, X. Quan, X. Fan, G. Yi, S. Chen, H. Yu, Y. Chen, Improving ion rejection of conductive nanofiltration membrane through electrically enhanced surface charge density, Environ. Sci. Technol. 53 (2019) 868–877.
[12] C. Hu, Z. Liu, X. Lu, J. Sun, H. Liu, J. Qu, Enhancement of the Donnan effect through capacitive ion increase using an electroconductive rGO–CNT nanofiltration membrane, J. Mater. Chem. A 6 (2018) 4737–4745.
[13] G. Yi, L. Du, G. Wei, H. Zhang, H. Yu, X. Quan, S. Chen, Selective molecular separation with conductive MXene/CNT nanofiltration membranes under electrochemical assistance, 658 (2022) 120719.
[14] S. Mareev, A. Gorobchenko, D. Ivanov, D. Anokhin, V. Nikonenko, Ion and water transport in ion-exchange membranes for power generation systems: guidelines for modeling, Int. J. Mol. Sci. 24 (1) (2023) 34.
[15] R.J. Gross, J.F. Osterle, Membrane transport characteristics of ultrafine capillaries, J. Chem. Phys. 49 (1968) 228–234.
[16] E.H. Cwirko, R.G. Carbonell, Transport of electrolytes in charged pores: analysis using the method of spatial averaging, J. Colloid Interface Sci. 129 (1989) 513–531.
[17] A. Szymczyk, B. Aoubiza, P. Fievet, J. Pagetti, Electrokinetic phenomena in homogeneous cylindrical pores, J. Colloid Interface Sci. 216 (1999) 285–296.
[18] P. Fievet, A. Szymczyk, C. Labbez, B. Aoubiza, C. Simon, A. Foissy, J. Pagetti, Determining the zeta potential of porous membranes using electrolyte conductivity inside pores, J. Colloid Interface Sci. 235 (2001) 383–390.
[19] I. Makra, G. Jágerszki, I. Bitter, R.E. Gyurcsányi, Nernst–Planck/Poisson model for the potential response of permselective gold nanopores, Electrochim. Acta 73 (2012) 70–77.
[20] P.M. Biesheuvel, M.Z. Bazant, Analysis of ionic conductance of carbon nanotubes, Phys. Rev. E. 94 (2016) 050601(R).
[21] P.B. Peters, R. van Roij, M.Z. Bazant, P.M. Biesheuvel, Analysis of electrolyte transport through charged nanopores, Phys. Rev. E 93 (2016) 053108.
[22] J. Catalano, H.V.M. Hamelers, A. Bentien, P.M. Biesheuvel, Revisiting Morrison and Osterle 1965 : the efficiency of membrane–based electrokinetic energy conversion, J. Phys.: Condens. Matter. 28 (2016) 324001.
[23] I.I. Ryzhkov, D.V. Lebedev, V.S. Solodovnichenko, A.V. Shiverskiy, M.M. Simunin, Induced-charge enhancement of diffusion potential in membranes with polarizable nanopores, Phys. Rev. Lett. 119 (2017) 226001.
[24] I.I. Ryzhkov, A.S. Vyatkin, E.V. Mikhlina, Modelling of conductive nanoporous membranes with switchable ionic selectivity, Membr. Membr. Technol. 2 (1) (2020) 10—19.
[25] I.I. Ryzhkov, M.A. Shchurkina, E.V. Mikhlina, M.M. Simunin, I.V. Nemtsev, Switchable ionic selectivity of membranes with electrically conductive surface: Theory and experiment, Electrochim. Acta 375 (2021) 137970.
[26] I.I. Ryzhkov, D.V. Lebedev, V.S. Solodovnichenko, A.V. Minakov, M.M. Simunin, On the origin of membrane potential in membranes with polarizable nanopores, J. Membr. Sci. 549 (2018) 616–630.
[27] M.Z. Bazant, T.M. Squires, Induced–charge electrokinetic phenomena, Curr. Opin. Colloid Interface Sci. 15 (2010) 203–213.
[28] J. Fuhrmann, C. Guhlke, A. Linke, C. Merdon, R. Müller, Induced charge electroosmotic flow with finite ion size and solvation effects, Electrochim. Acta 317 (2019) 778–785.
[29] J. Duval, G.K. Huijs, W.F. Threels, J. Lyklema, H.P. van Leeuwen, Faradaic depolarization in the electrokinetics of the metal–electrolyte solution interface, J. Colloid Interface Sci. 260 (2003) 95–106.
[30] L. Zhang, P.M. Biesheuvel, I.I. Ryzhkov, Theory of ion and water transport in electron–conducting membrane pores with pH–dependent chemical charge, Phys. Rev. Appl. 12 (2019) 014039.
[31] J. Duval, J. Lyklema, J.M. Kleijn, H.P. Van Leeuwen, Amphifunctionally electrified interfaces: coupling of electronic and ionic surface–charging processes, Langmuir 17 (2001) 7573–7581.
[32] J. Duval, M.J. Kleijn, J. Lyklema, H.P. Van Leeuwen, Double layers at amphifunctionally electrified interfaces in the presence of electrolytes containing specifically adsorbing ions, J. Electroanal. Chem. 532 (2002) 337–352.
[33] A.A. Kapitonov, I.I. Ryzhkov, Modelling the performance of electrically conductive nanofiltration membranes, Membranes 13 (2023) 596.
[34] P. Gao, C.R. Martin, Voltage charging enhances ionic conductivity in gold nanotube membranes, ACS Nano 8 (2014) 8266–8272.
[35] Q. Wang, C.S. Cha, J. Lu, L. Zhuang, Ionic conductivity of pure water in charged porous matrix, Chemphyschem 13 (2012) 514–519.
[36] D.V. Lebedev, V.S. Solodovnichenko, M.M. Simunin, I.I. Ryzhkov, Effect of electric field on ion transport in nanoporous membranes with conductive surface, Petrol. Chem. 58 (2018) 474–481.
[37] W. Guan, R. Fan, M.A. Reed, Field–effect reconfigurable nanofluidic ionic diodes, Nature Commun. 2 (2011) 506.
[38] T. Jain, B. Rasera, R. Guerrero, et al., Heterogeneous sub-continuum ionic transport in statistically isolated graphene nanopores, Nature Nanotechnology 10 (2015) 1053–1057.
[39] K. Yazda, S. Tahir, T. Michel, B. Loubet, M. Manghi, J. Bentin, F. Picaud, J. Palmeri, F. Henn, V. Jourdain, Voltage–activated transport of ions through single–walled carbon nanotubes, Nanoscale 9 (2017) 11976–11986.
[40] M. Tagliazucchi, I. Szleifer, Salt pumping by voltage–gated nanochannels, J. Phys. Chem. Lett. 6 (2015) 3534–3539.
[41] A.I. Krom, I.I. Ryzhkov, Ionic conductivity of nanopores with electrically conductive surface: Comparison between 1D and 2D models, Adv. Theory Simul. 4 (10) (2021) 2100174.
[42] J. Cervera, J.A. Manzanares, S. Mafé, Ion size effects on the current efficiency of narrow charged pores, J. Membr. Sci. 191 (2001) 179–187.
[43] I.I. Ryzhkov, A.V. Minakov, Finite ion size effects on electrolyte transport in nanofiltration membranes, J. Sib. Fed. Univ. Math. Phys. 10 (2) (2017) 186–198.
[44] I.I. Ryzhkov, I.A. Kharchenko, E.V. Mikhlina, A.V. Minakov, D.V. Guzei, I.V. Nemtsev, M.N. Volochaev, A.V. Korobko, M.M. Simunin, Growth of carbon nanotubes inside porous anodic alumina membranes: Simulation and experiment, Int. J. Heat Mass Transfer 176 (2021) 121414.
[45] M. Lillo, D. Losic, Pore opening detection for controlled dissolution of barrier oxide layer and fabrication of nanoporous alumina with through-hole morphology, J. Membr. Sci. 327 (2009) 11–17.
[46] Y. Tanaka, Chapter 7 concentration polarization, in: Ion Exchange Membranes - Fundamentals and Applications, 2007, pp. 97–138.
[47] N.A. Mishchuk, Concentration polarization of interface and non–linear electrokinetic phenomena, Adv. Colloid Interface Sci. 160 (2010) 16–39.
[48] A. Guirao, S. Mafé, J.A. Manzanares, J.A. Ibáñez, Biionic potential of charged membranes: Effects of the diffusion boundary layers, J. Phys. Chem. 99 (1995) 3387–3393.